INVITED PAPER *Special Section on Microwave and Millimeter-Wave Technologies*

A Review of GaN MMIC Power Amplifier Technologies for Millimeter-Wave Applications

Keigo NAKATANI[†a)], **Yutaro YAMAGUCHI**[†], **Takuma TORII**[†], ***Members***, ***and*** **Masaomi TSURU**[†], ***Senior Member***

SUMMARY GaN microwave monolithic integrated circuit (MMIC) power amplifiers (PAs) technologies for millimeter-wave (mm-wave) applications are reviewed in this paper. In the mm-wave band, GaN PAs have achieved high-output power as much as traveling wave tube amplifiers used in satellite communications. Additionally, GaN PAs have been integrated enough to be used for 5G and Beyond-5G. In this paper, a high accuracy large-signal GaN-HEMT modeling technique including the trapping effects is introduced in mm-waves. The prototyped PAs designed with the novel modeling technique have achieved RF performance comparable to that of the state-of-the-art GaN PAs in mm-wave.

key words: *GaN, SATCOM, 5G, high power amplifier, MMIC, Doherty amplifier, millimeter wave*

1. Introduction

In recent years, GaN technology is widely used in microwave applications and its operating frequency limit is expanding to millimeter-wave (mm-wave). In the satellite communication (SATCOM) systems, K and Ka-bands (18 to 40 GHz) are used to meet the demand for a high data rate [1], [2]. In 5G mobile systems [3], [4], a large system capacity, low latency, and massive connection will be provided for various applications according with 1000 times mobile traffic that is predicted in early 2020 compared with that of 2010. For this system, mm-wave massive multiple-input multiple-output (m-MIMO) is a promising technology [5]. Mm-wave 5G mobile systems, so called Frequency Range 2 (FR2), is expected to realize new communication services using large capacity and high throughput with the SATCOM [6].

Traveling wave tube amplifiers (TWTAs) are generally used as transmitters in mm-waves, because of their high power and high efficiency performances. On the other hand, it is difficult to satisfy highly linear operation for communication systems with wideband characteristics. The active phased array antenna systems with TWTAs require high power phase shifter and variable gain amplifier. It is not suitable for a transmitter that require small size [7]. GaN microwave monolithic integrated circuit (MMIC) power amplifiers (PAs) can play a major role in the high linear operation as well as circuit-size reduction and cost reduction of solid-state power amplifiers (SSPAs) by replacing conventional TWTAs in mm-waves.

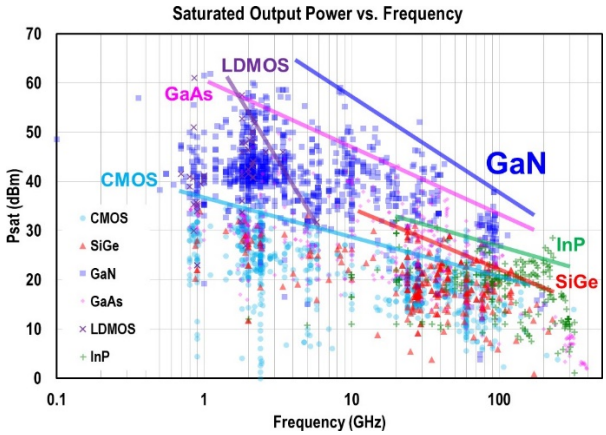

Fig. 1 Saturated output power vs. frequency of device technologies [8].

Figure 1 shows saturated output power versus frequency of device technologies [8]. The operating frequency of all devices is now extended, and the saturated output power is improved through the development of device technology. GaAs and silicon (Si) devices are generally used in relatively low output power applications. GaN devices have the advantage of high breakdown voltage for high output power and low output capacitance for high frequency operation. In addition, high thermal conductivity of SiC substrates allows GaN MMIC PAs to be implemented in small circuit size. GaN-based PAs also have the advantage of low distortion and wideband characteristics, compared to other technology devices. Consequently, GaN devices are well suited to high output power and high degree of integration required for SATCOM and 5G mobile systems in mm-waves.

This paper provides an overview of recent progress in GaN-HEMT modeling techniques and mm-wave GaN MMIC PAs for SATCOM and 5G mobile systems. Section 2 describes a large-signal GaN-HEMT model that incorporates trapping effects using an RC model and nonlinear capacitance. Section 3 presents the GaN MMIC PAs developed in K and Ka bands for the SATCOM system. In Sect. 4, the GaN Doherty MMIC PA developed for 5G mobile systems is described in detail. Finally, Sect. 5 concludes the paper.

Manuscript received January 28, 2022.
Manuscript revised March 1, 2022.
Manuscript publicized July 13, 2022.

[†]The authors are with Information Technology R&D Center, Mitsubishi Electric Corporation, Kamakura-shi, 247–8501 Japan.
a) E-mail: Nakatani.Keigo@cj.mitsubishielectric.co.jp

DOI: 10.1587/transele.2022MMI0006

2. Large Signal GaN-HEMT Modeling Technique in Mm-Wave

To design GaN MMIC PAs, a large-signal model of GaN high electron mobility transistor (GaN-HEMT) with a high accuracy is required. large-signal GaN-HEMT modeling techniques that take account of the trapping effects on the model as the drain current and transconductance have already been reported [9]–[11]. Additionally, it is important to take account of the trapping effects on the model as nonlinear capacitance in mm-wave band because it directly affects the amplitude modulation (AM) and phase modulation (PM) characteristics for SATCOM and 5G mobile systems amplifier design. In this section, a large-signal GaN-HEMT model that take account of the trapping effects on the model as nonlinear capacitance is described.

GaN-HEMT takes advantage of two-dimensional electron gas (2DEG) that is spontaneously formed between an aluminum gallium nitride (AlGaN) barrier and a GaN buffer. Figure 2 shows the simplified GaN-HEMT physical mechanisms of the proposed trap models under (a) direct current (DC) continuous condition and (b) DC pulsed condition [12]. Under the DC continuous condition, the gate is biased in the ON state, whereas the drain is continuously biased in the ON state under the low-voltage condition. However, in the pulsed condition, the gate and drain are immediately biased after the stress bias, which means that the gate voltage (V_g) is in the OFF state and the drain voltage (V_d) is high (30 to 50 V). The traps have a significant effect on the I-V and RF characteristics after stress bias because highly concentrated electrons are captured by traps owing to the strong electric field. As shown in Fig. 2, the drain current (I_d), gate-drain capacitance (C_{gd}), and drain-source resistance (R_{ds}) are strongly affected by the traps. That is, the acceptor-type traps at the GaN buffer layer are ionized by the capture of electrons after the stress bias; the concentration of 2DEG then decreases owing to the increased conduction band at the buffer layer. Consequently, I_d and C_{gd} decrease and R_{ds} increases. Additionally, the ionized trap region expands to the drain side because of the high V_d, and C_{gd} is considered to be more strongly affected by traps than the gate-source capacitance (C_{gs}).

Figure 3 shows a schematic of the proposed trap model. The Angelov-GaN model [13] was used as the fundamental large-signal model. As shown in Fig. 3, the trap circuit was loaded onto the drain terminal of the Angelov-GaN model. The trap circuit consists of a resistance (R_{trap}), capacitance (C_{trap}), and diode (D_{trap}). R_{trap} is a large value that prevents the drain current from flowing through the ground. When the voltage at the drain terminal is excited by a sine wave, as shown in Fig. 3, V_{btrap} is the only DC component in the half-wave rectifier of the sine wave. In other words, the trap circuit operates as a detector. When the amplitude of the drain voltage is increased under a large-signal operation, V_{btrap} also increases. V_{btrap} is fed back to C_{gd}, I_d, and g_m. Figures 4 a and 4 b show the AM-AM and AM-PM characteristics at 28 GHz, respectively, to verify the proposed model. The dotted line represents the measured results, the solid line represents the simulated results using the proposed model, and the dotted line represents the simulated results using the conventional model. The conventional model is a general large-signal GaN-HEMT model that does not take account of the trapping effects on nonlinear capacitance. Therefore, the accuracy of AM-AM and AM-PM at saturated output operation is not good. As shown in Fig. 4, the proposed model is in good agreement with the measurements in both AM-AM and AM-PM characteristics.

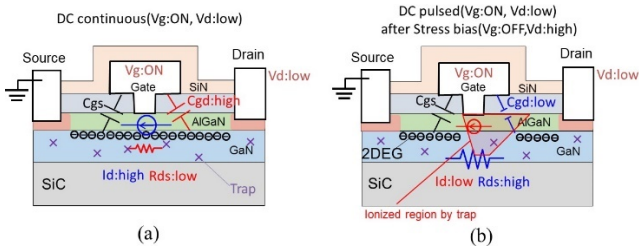

Fig. 2 Simplified GaN-HEMT physical mechanisms of the proposed trap models under (a) DC continuous condition; and (b) DC pulsed condition [12].

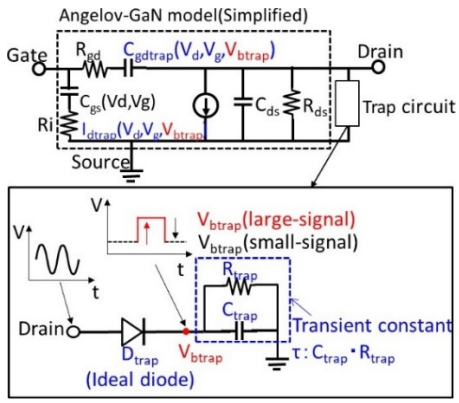

Fig. 3 Schematic of the proposed trap model [12].

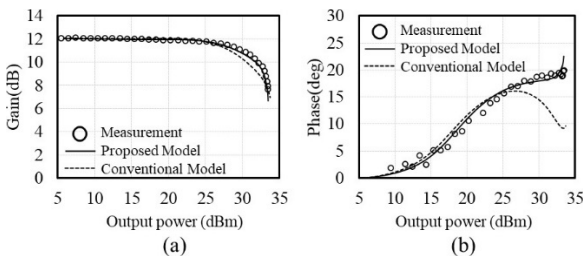

Fig. 4 Measured and simulated results of large-signal characteristics. (a) AM-AM, (b) AM-PM [12].

3. GaN MMIC PA Technology Trend in K and Ka-Band for SATCOM System

Three GaN MMIC PAs that can be applied to the SATCOM system in the K and Ka-bands are described. Ta-

Table 1 Frequency Band of the SATCOM system

SATCOM Frequency Band	Frequency Range	Band Width	Output Power/ PA	Application
K-Band	17.3 – 21.2 GHz	3.9 GHz	> 10 W	SATCOM downlink
Ka-Band	27.5 – 31.0 GHz	3.5 GHz	> 10 W	SATCOM uplink

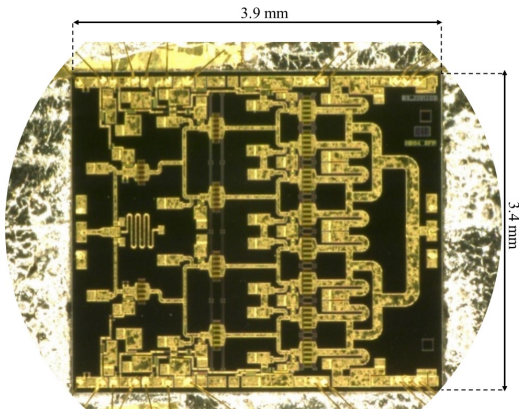

Fig. 5 Chip photograph of the fabricated K-band GaN MMIC PA [18].

ble 1 lists the frequency bands of the SATCOM system. The SATCOM system is classified in two frequency bands, (a) 17.3 to 21.2 GHz (K-band) for downlink, fixed satellite services and broadcast satellite services, (b) 27.5 to 31.0 GHz (Ka-band) for uplink, SATCOM and 5G mobile systems. The GaN MMIC PA solution offers competitive advantages, because it can achieve a high linearity operation with wideband characteristics and high accuracy control of phase and amplitude far above the TWTAs. The transmitter modules of SSPAs consist of multiple PAs. In order to reduce the size of transmitter module, a PA with a high output power density and high efficiency is required. GaN MMIC PAs meet the demand for both a small size and the high output power. However, an efficiency of GaN MMIC PAs has a trade-off relationship with the output power of that caused by a loss of inner power combiner networks, and the efficiency requirements depends on specifications of each SSPAs which is derived considering their thermal managements. In this section, GaN MMIC PAs with several output powers are introduced. First, a high output power K-band GaN MMIC PA compared with reported PAs [14]–[17] is described [18]. Second, 15 W and 32 W high output power density Ka-band GaN MMIC PAs compared with reported PAs [19]–[22] are explained [23], [24]. A high accuracy GaN-HEMT model is useful to design several output powers GaN MMIC PAs in a short term.

The GaN MMIC PA was fabricated utilizing a 0.15 μm gate length GaN process on a 50 μm thick SiC substrate with Individual Source Via (ISV) structure. Figure 5 shows a chip photograph of the fabricated K-band GaN MMIC PA [18]. The GaN MMIC PA consists of 3 stage Class-AB PAs. The number of gate fingers of the unit FET cell was 10 with unit gate width of 80 μm for the final stage. The final stage contained 8 FET cells, and 4 FET cells and 2 FET cells were

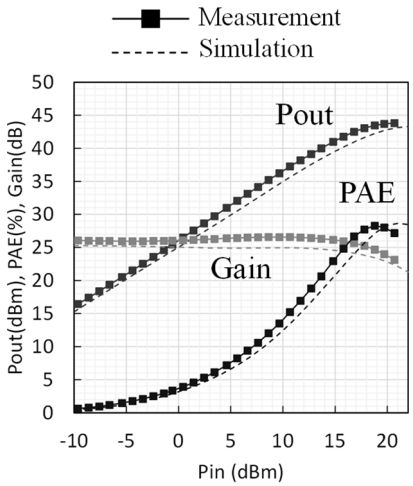

Fig. 6 Measured and simulated results of the input-output characteristics under continuous wave condition [18].

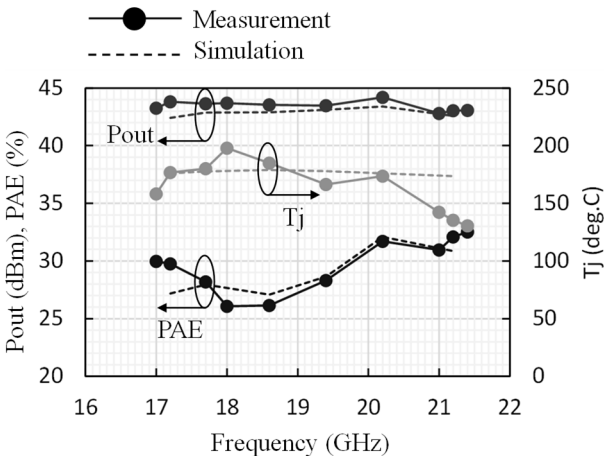

Fig. 7 Measured performance over frequency [18].

used for the 2nd and 1st driver stage. Figure 6 shows the measured and simulated results of the input-output characteristics under continuous wave condition. The measured results were in good agreement with the simulated results. A maximum output power of 44.2 dBm (26 W) and maximum PAE of 32% were achieved with a power gain of over 25 dB at the best performing frequency. Figure 7 shows the measured performance over frequency. The junction temperature was estimated based on the calculated thermal resistance and the dissipation power was estimated based on the measured results of the output power and drain current of each stage. The junction temperature was approximately 170°C, which corresponded well with the simulated result. For wideband operation, the power amplifier realized an output power of 42.8 dBm (19 W), a PAE of over 26%, and a power gain of 25 dB over 17 to 21.4 GHz. Figure 8 shows the measurement results of adjacent channel power ratio (ACPR) and error vector magnitude (EVM). A modulation signal of 8-PSK (roff = 0.15, bandwidth = 10 MHz) was applied as a test signal, and a peak to average ratio (PAPR) of approxi-

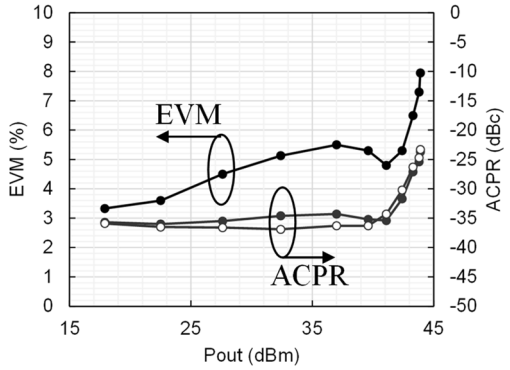

Fig. 8 Measured results of ACPR and EVM [18]

Table 2 State-of-the-art of a K-band GaN power amplifiers

Ref	Freq (GHz)	FBW (%)	Num. stage	Pout (dBm)	PAE (%)	Gain (dB)
[14]	17.2 – 20.2	16.0	2	41 – 42	36 – 43	17
[15]	17 – 20	16.2	3	40 – 42	30 – 36	25
[16]	17 – 21	21.1	2	40	36 – 40	22
[17]	17 – 20.2	17.2	3	40 – 41	30 – 36	22.5
this work	17.2 – 21.2	20.8	3	42.8 – 44.2	26 – 32	25

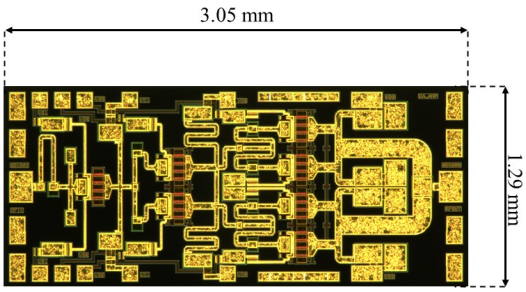

Fig. 9 Chip photograph of the 15 W Ka-band GaN MMIC PA [23].

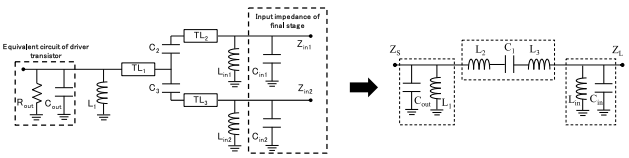

Fig. 10 Proposed ISMN using the BPF configuration [23].

mately 8.4 dB. An average output power of 42.4 dBm, PAE of 28.9%, gain of 26.5 dB, EVM of 5.4%, and ACPR of −30 dBc were achieved. Table 2 shows the state-of-the-art of K-band GaN power amplifiers. The output power of the fabricated power amplifier is comparatively higher than other reported K-Band GaN MMIC PAs.

The Ka-band GaN MMIC PAs were also fabricated by the 0.15 μm gate length GaN process on a 50 μm thickness SiC substrate with the ISV structure. Figure 9 shows the chip photograph of the 15 W Ka-band GaN MMIC PA [23]. The GaN MMIC PAs consist of three stage Class-AB PAs. The number of gate finger of the unit FET cell was 8 with a 70 μm unit gate width for each stage. For the final stage, 4 FET cells were combined. Figure 10 shows the proposed inter stage matching network (ISMN) using the band-pass filter (BPF) configuration. The proposed ISMN consists of shunt inductors (L1, Lin1, Lin2), series capacitors (C2, C3) and transmission lines (TL4, TL5, TL6). The proposed ISMN divides an output transistor impedance of driver stage into two of input transistor impedance of the final stage. These circuit elements can be modified as an equivalent circuit of Butterworth BPF circuits. The proposed ISMN is designed with including the parasitic capacitances of the transistors for the final and driver stages. Figure 11 shows the simulated results of the proposed ISMN and a conventional ISMN using low-pass filter (LPF) configuration. The insertion loss of the proposed ISMN is lower than that of the conventional ISMN. Moreover, the proposed ISMN provides wider frequency response than the conventional ISMN. Consequently, a high efficiency and wideband Ka-band GaN MMIC PA was realized by applying the proposed ISMN. Figure 12 shows the measured input-output characteristics of 15 W GaN MMIC PA. The measured maximum output power of 41.8 dBm, peak PAE of 31% and gain of 21 dB were obtained under pulse operation (pulse period = 1 ms, pulse duty = 10%) in 28 GHz. Figure 13 shows the measured performance over frequency. The measured maximum output power of 41.0 to 41.8 dBm and a peak PAE of

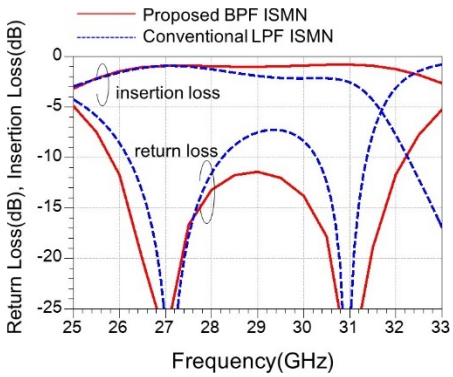

Fig. 11 Simulated results of the proposed ISMN and a conventional ISMN using LPF configuration [23].

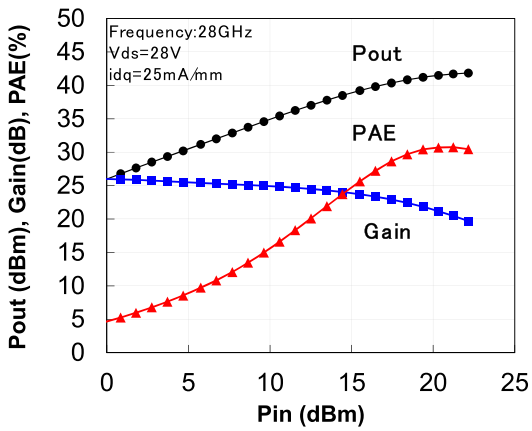

Fig. 12 Measured input-output characteristics of 15 W GaN MMIC PA [23].

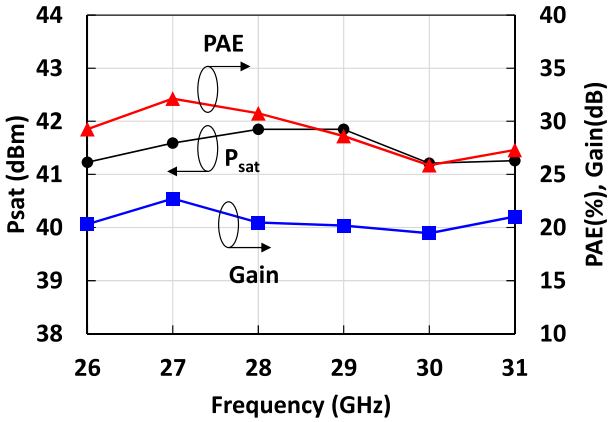

Fig. 13 Measured performance over frequency [23].

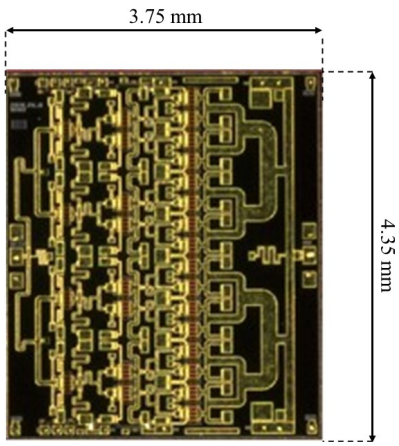

Fig. 14 Chip photograph of a 40 W Ka-band GaN MMIC PA [24].

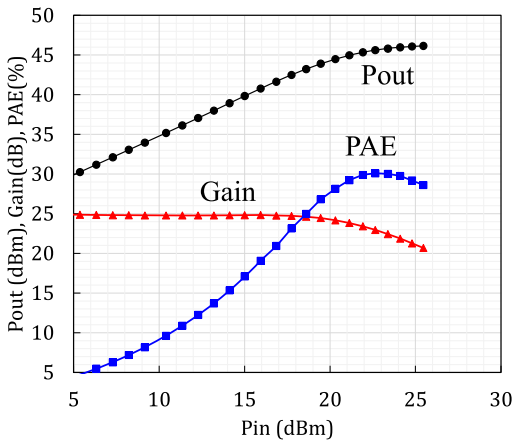

Fig. 15 Measured input-output characteristics of the 40 W GaN PA [24].

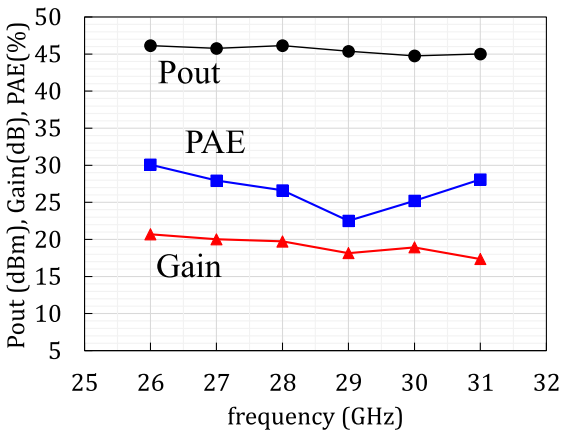

Fig. 16 Measured performance over frequency [24].

27 to 32% and gain of 20.0 to 22.0 dB were obtained over 26 to 31 GHz (FBW = 17.5%).

The output power of the Ka-band GaN MMIC PA shown in Fig. 9 is sufficient for replacing the TWTAs. There is a requirement for higher output power GaN MMIC PAs. Figure 14 shows a chip photograph of a 40 W Ka-band GaN MMIC PA [24]. The number of gate finger of the unit FET cell was 8 with a 80 μm unit gate width for each stage. In order to achieve high output power, 16 FET cells were combined at the final stage. The total gate width of this GaN MMIC PA approximately four times than that of the PA shown in Fig. 9. Figure 15 shows the measured input-output characteristics of the 40 W GaN MMIC PA. A measured maximum output power of 46.2 dBm, peak PAE of 30.2%, and gain of 18 dB were obtained under pulse operation (pulse period = 1 ms, pulse duty = 10%) at 28 GHz. Figure 16 shows the measured performance over frequency. The measured maximum output power of 45.0 to 46.2 dBm (31.6 to 41.7 W) and peak PAE of 23 to 30.2% and gain of 17.4 to 20.7 dB were obtained over 26 to 31 GHz (FBW = 17.5%). Table 3 shows the state-of-the-art of a Ka-band GaN MMIC PA. The two fabricated Ka-band GaN MMIC PAs achieved high output power density with high efficiency. The prototype of GaN MMIC PAs demonstrated output power of over 10 W with high efficiency at both K and Ka-bands required in the SATCOM system.

Table 3 State-of-the-art of a Ka-band GaN power amplifiers.

Ref	Freq (GHz)	FBW (%)	Num. stage	Pout (dBm)	PAE (%)	Pd (W/mm^2)
[19]	27 - 31	13.8	3	39.0	34.7	2.02
[20]	27.5 - 31	12.0	3	42.1	42.5	2.32
[21]	26 - 30	13.8	2	46	36	2.94
[22]	26.5 - 31	15.7	3	46.2	25.9	2.37
this work [23]	26 - 31	17.5	3	41.8	32	3.85
this work [24]	26 - 31	17.5	3	46.2	30.2	2.56

4. GaN MMIC PA Technology Trend in 5G Mm-Wave System

As mentioned in the Sect. 1, the Ka-band is also used in mm-wave 5G mobile systems. The base transceiver stations (BTSs) are classified into three categories depending on the equivalent isotropic radiation power (EIRP): (a) short range BTSs, which is used for in-room or hot spot high speed wireless connections, whose EIRP is less than 50 dBm; (b) middle range BTSs for high density urban areas and urban macro, whose EIRP is 50 to 60 dBm; and (c) long range

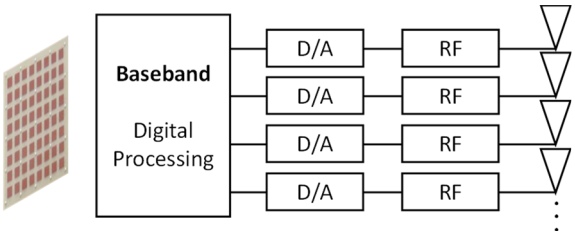

Fig. 17 All-digital beamforming antenna system [27].

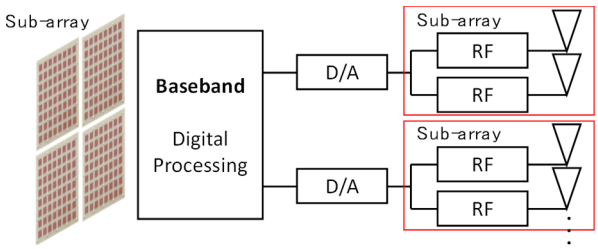

Fig. 18 Sub-array hybrid-beamforming antenna system [27].

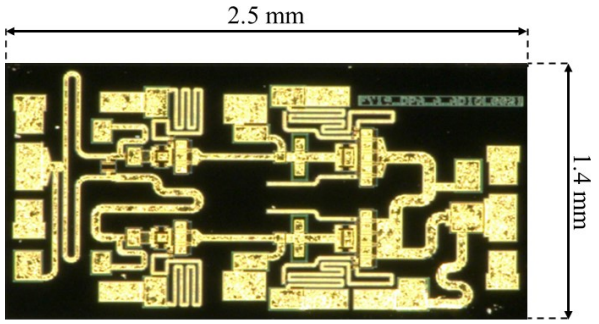

Fig. 19 Chip photograph of the GaN doherty MMIC PA [31].

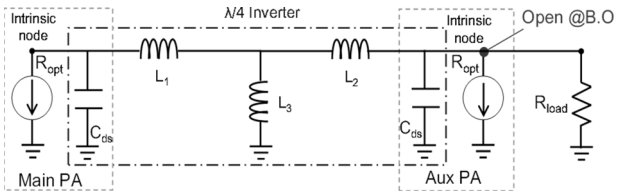

Fig. 20 Schematic of the Tee-network impedance inverter [31].

BTSs, which is used for wireless back-haul connections in rural areas, whose EIRP is 60 to 70 dBm. For short range BTSs, an integrated silicon RF-IC solution is advantageous because it is generally inexpensive [25]. For the middle range BTSs, the GaAs MMIC solution can be used because the output power of the GaAs MMIC is 10 to 15 dB higher than that of silicon RF-ICs. For long range BTSs, a GaN solution is more likely to be adopted because its output power is far above that of the silicon RF-IC or GaAs MMIC [26].

Two types of beamforming antenna systems exist, as shown in Fig. 17 and Fig. 18. BTSs vendors have been considering expanding their sub-6 all-digital beamforming antenna system to be applied to mm-wave 5G mobile systems. An all-digital beamforming antenna system can realize many functions and high-accuracy control of massive multiple-input multiple-output beamforming. However, owing to the drastic increase in the channel bandwidth in mm-waves and the need for many active channel elements, there is a problem of power dissipation and cost. Therefore, BTSs vendors have proposed a sub-array hybrid-beamforming antenna system that combines analog and digital beamforming techniques [27]. It combines digital precoding and analog beamforming to simultaneously generate multiple beams in a single space, which allows flexibility between the number of baseband channels and the number of active RF channels. However, a sub-array hybrid-beamforming antenna system requires higher output power in Tx transmitter than all-digital beamforming Tx transmitter due to divide a Tx channel into multiple Tx channels. Therefore, high output power and high integrated transmitter is required to realize hybrid-beamforming antenna system.

Doherty power amplifier (DPA) technology has been used since 3G, 4G, and sub-6 5G BTSs, and new types of DPAs have been proposed [28]–[30]. However, it is difficult to achieve high efficiency and wideband characteristics owing to the large influence of parasitic elements in the mm-wave band. The frequency response of Doherty circuit configuration is limited by loaded Q factor which is derived from output impedance and output parasitic capacitance of transistors. In order to achieve high efficiency and wideband characteristics in mm-waves, Doherty circuit configuration that compensates output parasitic capacitance is required.

Figure 19 shows the chip photograph of the GaN Doherty MMIC PA, which was fabricated by the 0.15 μm gate length GaN process on the 50 μm thickness SiC substrate with the ISV structure [31]. Figure 20 shows the schematic of the impedance inverter formed by the Tee-network for the output combiner of the fabricated DPA. The Tee-network is formed by the L_1, L_2, L_3 and C_{ds} of each transistor output parasitic capacitance. It operates as Doherty load modulation circuit by forming a impedance inverter. Figure 21 shows the measured (a) PAE and (b) Gain of fabricated DPA. As shown in Fig. 21, it was confirmed that the amplifier maintains the operation as a DPA in the wideband of 26 to 30 GHz. The DPA obtained output power of 36.1 to 36.5 dBm, a 6 dB and 8 dB output power back-off (OBO) PAE of 25 to 27%, 20.4 to 24.5%, and a peak PAE of 26.7 to 31.8%. To evaluate the linearity of the DPA, the ACPR and EVM were measured using the 64-QAM 45 MHz modulated signal with PAPR of 9.2 dB. Figure 22 shows the measured ACPR, EVM, and PAE over the frequency at average output power of 28 dBm. In the frequency of 26 to 30 GHz, the DPA achieved an ACPR lower than −27 dBc, EVM of 3.2 to 5.0%, and PAE of 20.1 to 23.8% at Pave = 28 dBm. Table 4 shows comparison with the state-of-the-art of Ka-band GaN DPAs. To the best of authors' knowledge, the performance of the fabricated DPA in this work is the widest bandwidth with the high efficiency in Ka-band.

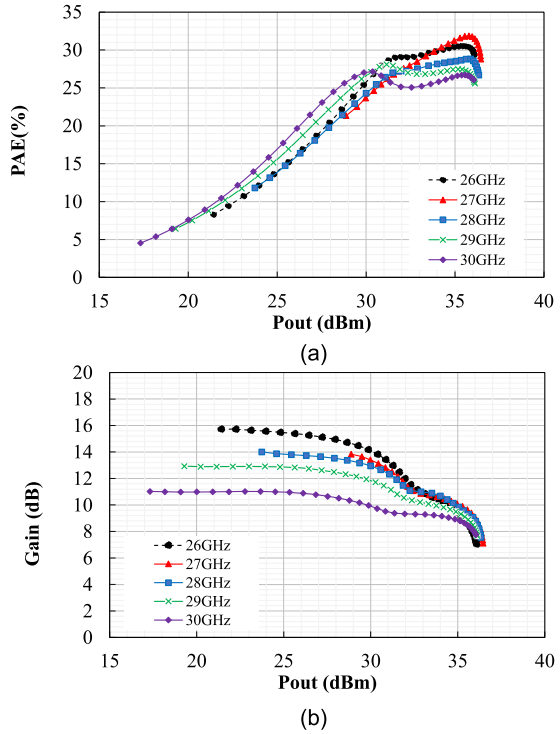

Fig. 21 Measured PAE and Gain of fabricated DPA [31].

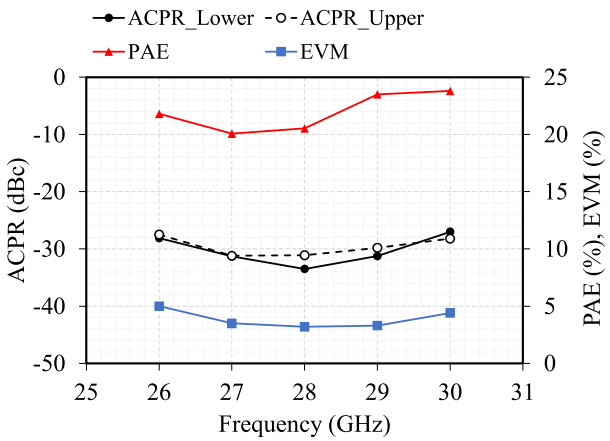

Fig. 22 Measured ACPR, EVM, and PAE [31]

Table 4 State-of-the-art of a Ka-band Doherty GaN power amplifiers.

Reference	Number of stages	Frequency (GHz)	FBW (%)	PAE at 6dB B.O. (%)	Peak PAE (%)	Pout (dBm)	Chip size (mm^2)	Power density (W/mm^2)
[32]	2	27.5-29.5	7	17-22.7	22.5-25.5	35.6	4.3	0.84
[33]	2	27-29.5	8.8	23-34	16-30	29-32	6.0	0.26
[34]	3	27-29.5	8.8	20-24	22-30	39	9.7	0.82
This work	2	26-30	14.6	25-27	26.7-31.8	36.1-36.5	3.5	1.14

5. Conclusion

This paper provides an overview of advances in a high accuracy large-signal GaN-HEMT modeling technique and GaN MMIC PAs for mm-wave applications on the basis of several published papers. The prototyped GaN PAs designed with the novel modeling technique has achieved good performances which are suitable to high power and high integration requirements of SATCOM and 5G mobile systems in mm-waves.

References

[1] M. Giordani and M. Zorzi, "Satellite Communication at Millimeter Waves: a Key Enabler of the 6G Era," IEEE International Conference on Computing, Networking and Communications (ICNC), Feb. 2020.
[2] https://www.soumu.go.jp/main_content/000593247.pdf
[3] https://www.oulu.fi/6gflagship/
[4] https://www.nttdocomo.co.jp/english/corporate/technology/whitepaper_6g/
[5] S. Shinjo, K. Nakatani, K. Tsustumi, and H. Nakamizo, "Integrating the Front End: A Higly Integrated RF Front End for High-SHF Wide-Band Massive MIMO in 5G," IEEE Microwave Magazine, vol.18, no.5, pp.21–40, 2017.
[6] H. Saarnisaari and C.M. de Lima, "5G New Radio in SATCOM: An overview of physical and medium access layer issues," in Proc. 22nd Int. Conf. Transparent Opt. Nets (ICTON), pp.1–4, 2020.
[7] J.P. Choi and V.W.S. Chan, "Resource management for advanced transmission antenna satellites," IEEE Trans. Wireless Commun., vol.8, no.3, pp.1308–1321, March 2009.
[8] H. Wang, T-Y. Huang, N.S. Mannem, J. Lee, E. Garay, D. Munzer, E. Liu, Y. Liu, B. Lin, M. Eleraky, H. Jalili, J. Park, S. Li, F. Wang, A.S. Ahmed, C. Snyder, S. Lee, H.T. Nguyen, and M.E.D. Smith, "Power Amplifiers Performance Survey 2000-Present," [Online]. Available: https://gems.ece.gatech.edu/PA_survey.html.
[9] Y. Tang, K. Shinohara, D. Regan, A. Corrion, D. Brown, J. Wong, A. Schmitz, H. Fung, S. Kim, and M. Micovic, "Ultrahigh-speed GaN high-electron-mobility transistors with f_T/f_{max} of 454/444 GHz," IEEE Electron Device Lett., vol.36, no.6, pp.549–551, June 2015.
[10] Y. Yamaguchi, J. Kamioka, M. Hangai, S. Shinjo, and K. Yamanaka, "A CW 20 W Ka-band GaN high power MMIC amplifier with a gate pitch designed by using one-finger large signal models," 2017 IEEE Compound Semiconductor IC Symposium, pp.309–312, 2017.
[11] O. Jardel, F. De Groote, C. Charbonniaud, T. Reveyrad, J.P. Teyssier, R. Quere, and D. Floriot, "A Drain-lag Model for AlGaN/GaN Power HEMTs," Microwave Symposium, 2007, IEEE/MTT-S International, pp.601–604, June 2007.
[12] Y. Yamaguchi, T. Otsuka, M. Hangai, S. Shinjo, and T. Oishi, "Ka-Band GaN Large-Signal Model Considering Trap Effect on Nonlinear Capacitance by Using Transient S-Parameters Measurement," 2018 IEEE BiCMOS and Compound Semiconductor Integrated Circuits and Technology, 2018.
[13] I. Angelov, V. Desmaris, K. Dynefors, P.A. Nilsson, N. Rorsman, H. Zirath, "On the large-signal modeling of AlGaN/GaN HEMTs and SiC MESFETs," Gallium Arsenide and Other Semiconductor Application Symposium 2005, pp.309–312, May 2005.
[14] S. Din, A.M. Morishita, N. Yamamoto, C. Brown, M. Wojtowicz, and M. Siddiqui, "High-power K-band GaN PA MMICs and module for NPR and PAE," IEEE MTT-S Int. Microw. Symp. Dig., pp.1838–1841, 2017.
[15] https://www.qorvo.com/products/p/TGA4548
[16] L. Marechal, M. Dinari, T. Huet, E. Richard, V. Serru, M. Camiade, C. Chang, L. Brunel, G. Mouchon, B. Gerfault, and G.L. Rhun, "10 W K band GaN MMIC amplifier embedded in Waveguide-based Metal Ceramic Package," 2019 14th European Microwave Integrated Circuits Conference (EuMIC), pp.184–187, 2019.
[17] P. Colantonio and R. Giofré, "A GaN-on-Si MMIC Power Amplifier with 10 W Output Power and 35% Efficiency for Ka-Band Satellite Downlink," 2020 15th European Microwave Integrated Circuits Conference (EuMIC), Utrecht, Netherlands, pp.29–32, 2021, doi: 10.1109/EuMIC48047.2021.00019.

[18] T. Torii, Y. Kawamura, E. Kuwata, and M. Tsuru, "A K-Band 25 W Class and High Gain GaN Power Amplifier for Satellite Communication," The Institute of Electronics, Information and Communication (IEICE), C-2-3, 2021.
[19] https://www.qorvo.com/products/p/QPA2210D
[20] https://www.qorvo.com/products/p/QPA2211D
[21] S. Din, M. Wojtowicz, and M. Siddiqui, "High power and high efficiency Ka band power amplifier," in 2015 IEEE MTT-S International Microwave Symposium, pp.1–4, May 2015.
[22] M. Roberg, T.R.M. Kywe, M. Irvine, O. Marrufo, and S. Nayak, "40 W Ka-Band Single and Dual Output GaN MMIC Power Amplifiers on SiC," in Comp. Semicond. Integr. Circuits Techn. Symp. (BCICTS), IEEE, pp.140–143, 2018.
[23] K. Nakatani and S. Shinjo, "Advanced GaN Power Amplifier MMICs for Millimeter-Wave Applications," European Microwave Week 2020 (EuMW2020) Workshop, W-11, 2021.
[24] K. Nakatani, Y. Yamaguchi, and M. Tsuru, "A Ka-Band 40 W GaN MMIC Power Amplifier for SATCOM," The Institute of Electronics, Information and Communication (IEICE), C-2-2, 2021.
[25] R. McMorrow, D. Corman, and A. Crofts, "All silicon mmW planar active antennas: The convergence of technology, applications, and architecture," 2017 IEEE International Conference on Microwaves, Antennas, Communications and Electronic Systems (COMCAS) 2017.
[26] S. Shinjo, K. Nakatani, J. Kamioka, R. Komaru, H. Noto, H. Nakamizo, S. Yamaguchi, S. Uchida, A. Okazaki, and K. Yamanaka. "A 28 GHz-band highly integrated GaAs RF frontend Module for Massive MIMO in 5G," In 2018 IEEE MTT-S International Microwave Workshop Series on 5G Hardware and System Technologies (IMWS-5G), pp.1–3. IEEE, 2018
[27] X. Liu, Q. Zhang, W. Chen, H. Feng, L. Chen, F.M. Ghannouchi, and Z. Feng, "Beam-Oriented Digital Predistortion for 5G Massive MIMO Hybrid Beamforming Transmitters," in IEEE Transactions on Microwave Theory and Techniques, vol.66, no.7, pp.3419–3432, July 2018.
[28] Y. Komatsuzaki, K. Nakatani, S. Shinjo, S. Miwa, R. Ma, and K. Yamanaka, "3.0–3.6 GHz wideband, over 46% average efficiency GaN Doherty power amplifier with frequency dependency compensating circuits," 2017 IEEE Topical Conference on RF/Microwave Power Amplifiers for Radio and Wireless Applications (PAWR), p.22, 2017.
[29] S.Y. Komatsuzaki, R. Ma, M. Benosman, Y. Nagai, S. Sakata, K. Nakatani, and S. Shinjo, "A Novel 1.4–4.8 GHz Ultra-Wideband, over 45% High Efficiency Digitally Assisted Frequency-Periodic Load Modulated Amplifier," 2019 IEEE MTT-S International Microwave Symposium (IMS), p.706, 2019.
[30] K. Nakatani, Y. Yamaguchi, Y. Komatsuzaki, S. Sakata, S. Shinjo, and K. Yamanaka, "A Ka-band high efficiency doherty power amplifier MMIC using GaN-HEMT for 5G application," in IEEE MTT-S Int. Microw. Symp. Dig., pp.1–3, Aug. 2018. doi: 10.1109/IMWS-5G.2018.8484612.
[31] Y. Yamaguchi, K. Nakatani, and S. Shinjo, "A Wideband and High Efficiency Ka-band GaN Doherty Power Amplifier for 5G Communications," 2020 IEEE BiCMOS and Compound Semiconductor Integrated Circuits and Technology Symposium (BCICTS), 2021.
[32] K. Nakatani, Y. Yamaguchi, Y. Komatsuzaki, S. Sakata, S. Shinjo, and K. Yamanaka, "A Ka-Band High Efficiency Doherty Power Amplifier MMIC using GaN-HEMT for 5G Application," IEEE MTT-S International Microwave Workshop Series on 5G Hardware and System Technologies (IMWS-5G), Aug. 2018.
[33] R. Giofre, A.D. Guadio, and E. Limiti, "A 28 GHz MMIC Doherty Power Amplifier in GaN on Si Technology for 5G Applications," IEEE MTT-S International Microwave Symposium (IMS), June 2019.
[34] D. Wohlert, B. Peterson, T.R.M. Kywe, L. Ledezma, and J. Gengler, "8-Watt Linear Three-Stage GaN Doherty Power Amplifier for 28 GHz 5G Applications," IEEE BiCMOS and Compound semiconductor Integrated Circuits and Technology Symposium (BCICTS), Nov. 2019.

Keigo Nakatani received his B.S. and M.S. degrees in Science and Technology from Ryukoku University in 2013 and 2015, respectively. In 2015, he joined the Information Technology Research and Development Center, Mitsubishi Electric Corporation, Kanagawa, Japan, where he has been engaged in the research and development of GaN power amplifiers and microwave monolithic integrated circuits.

Yutaro Yamaguchi received his B.E. and M.E. degrees in Electrical Engineering from the Tokyo Institute of Technology in 2009 and 2011, respectively. In 2011, he joined the Information Technology Research and Development Center, Mitsubishi Electric Corporation, Kanagawa, Japan, where he has been engaged in the research and development of GaN device modeling and microwave high-power amplifiers.

Takuma Torii received his BE and ME degrees from the Tokyo University of Science, Tokyo, Japan, in 2012 and 2016, respectively. He joined Mitsubishi Electric Corporation in 2014. Since 2015, he has been engaged in research on Ku-band power amplifiers at the Mitsubishi Electric Information Technology R&D Center. He is a member of IEICE.

Masaomi Tsuru received his B.S. and M.S. degrees in electronic engineering from the Kyushu Institute of Technology, Fukuoka, Japan, in 1996 and 1998, respectively, and his Dr. Eng. Degree from Tohoku University, Sendai, Japan, in 2016. He joined Mitsubishi Electric Corporation, Kanagawa, Japan, in 1998, where he has been engaged in the research and development of microwave and millimeter-wave oscillators for radar and communication systems, millimeter-wave RF frontend ICs for communication systems, and rectifiers for microwave power transmission systems. He was a recipient of the 2004 Young Engineer Award presented by the Institute of Electronics, Information and Communication Engineers (IEICE), Japan, the 2009 IEEE MTT-S Japan/Kansai Chapters' Young Engineer Award, and the 2009 Michiyuki Uenohara Memorial Award.